JACS
JOURNAL OF THE AMERICAN CHEMICAL SOCIETY

Article

pubs.acs.org/JACS

Self-Assembled Molecular Rafts at Liquid|Liquid Interfaces for Four-Electron Oxygen Reduction

Astrid J. Olaya,[†] Delphine Schaming,[†] Pierre-Francois Brevet,[‡] Hirohisa Nagatani,[§] Tomas Zimmermann,[∥] Jiri Vanicek,[∥] Hai-Jun Xu,[⊥] Claude P. Gros,[⊥] Jean-Michel Barbe,[⊥] and Hubert H. Girault*[,†]

[†]Laboratoire d'Electrochimie Physique et Analytique, Station 6, Ecole Polytechnique Fédérale de Lausanne, CH-1015 Lausanne, Switzerland

[‡]Laboratoire de Spectrométrie Ionique et Moléculaire, UMR CNRS 5579, Université Claude Bernard Lyon 1, 43 Bd du 11 Novembre 1918, 69622 Villeurbanne cedex, France

[§]Faculty of Chemistry, Institute of Science and Engineering, Kanazawa University, Kakuma, Kanazawa 920-1192, Japan

[∥]Laboratory of Theoretical Physical Chemistry, Institut des Sciences et Ingénierie Chimiques, Ecole Polytechnique Fédérale de Lausanne, CH-1015 Lausanne, Switzerland

[⊥]Institut de Chimie Moléculaire de l'Université de Bourgogne, ICMUB (UMR 5260, CNRS), France

Supporting Information

ABSTRACT: The self-assembly of the oppositely charged water-soluble porphyrins, cobalt tetramethylpyridinium porphyrin ($CoTMPyP^{4+}$) and cobalt tetrasulphonatophenyl porphyrin ($CoTPPS^{4-}$), at the interface with an organic solvent to form molecular "rafts", provides an excellent catalyst to perform the interfacial four-electron reduction of oxygen by lipophilic electron donors such as tetrathiafulvalene (TTF). The catalytic activity and selectivity of the self-assembled catalyst toward the four-electron pathway was found to be as good as that of the Pacman type cofacial cobalt porphyrins. The assembly has been characterized by UV−visible spectroscopy, Surface Second Harmonic Generation, and Scanning Electron Microscopy. Density functional theory calculations confirm the possibility of formation of the catalytic $CoTMPyP^{4+}$/ $CoTPPS^{4-}$ complex and its capability to bind oxygen.

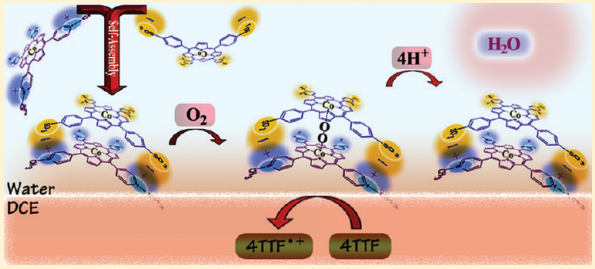

1. INTRODUCTION

The catalytic four-electron reduction of oxygen in aqueous acidified media is a key step in the development of fuel cells and batteries. The electrocatalysts generally used are based on precious metals nanoparticles supported on high area carbon materials. These are, however, expensive and can produce H_2O_2 as a side product with deleterious effects.[1] Organic complexes of transition metals like porphyrins are attractive systems for the development of biomimetic catalysts, since in aerobic organisms, the four-electron reduction of oxygen is carried out by membrane bound enzymes containing a porphyrin substructure as the catalyst.[1−5] For example, several synthetic bis-(cobalt)-substituted diporphyrins adsorbed onto the edge plane of pyrolytic graphite electrodes (EPG) have been studied for dioxygen reduction; between them, face-to-face diporphyrins [Co_2(FTF4)] and the Pacman type porphyrins [Co_2(DPA)], [Co_2(DPB)], and [Co_2(DPX)] (DiPorphyrins (DP) with anthracenyl (A), biphenylenyl (B), and xanthenyl (X) bridges) have shown a good selectivity toward the formation of H_2O, about 100% for the double bridged [Co_2(FTF4)] and 80% for the single bridged Pacman porphyrins.[1,5−8] Alternatively, cobalt-(II) tetraphenylporphyrin trapped in a thin layer-conducting polymer, deposited on an indium tin oxide (ITO) electrode, has also shown high selectivity toward the four-electron reduction.[9] More recently, "Hangman" porphyrins with specific functional groups adjusting the pK_a of dioxygen adducts to promote proton-coupled multielectron transfer reactions have shown a selectivity of about 50%.[3]

The development of supramolecular assemblies of porphyrins is being actively pursued to enhance or taylor the properties of porphyrins, and therefore, is an attractive subject in many fields of research.[10−14] Self-assembled porphyrins can be obtained by electrostatic attractions between two oppositely charged substituted porphyrins, by intermolecular $\pi-\pi$ stacking interactions, chemical linkage or covalent binding[10−14] yielding different structures such as particles, tubes, rods, cubes, spheres, clovers-like, etc.[10−18]

The Interface between Two Immiscible Electrolyte Solutions (ITIES) is a useful system to study processes involved in biocatalysis, ion pumping or photosynthesis among others.[19−22] Oxygen reduction by lipophilic electron donors such as ferrocene (Fc)[19−23] and decamethylferrocene (DMFc),[19,22−24] and mediated by cobalt porphyrins as catalysts at the water |1,2 dichloroethane interface has been studied.[19,21] In most cases the selectivity toward the four-electron reduction has been low. Recently,

Received: September 16, 2011
Published: November 22, 2011

Scheme 1. Diagram of the Optical Setup Used for the SSHG Measurements at the Liquid|Liquid Interfaces

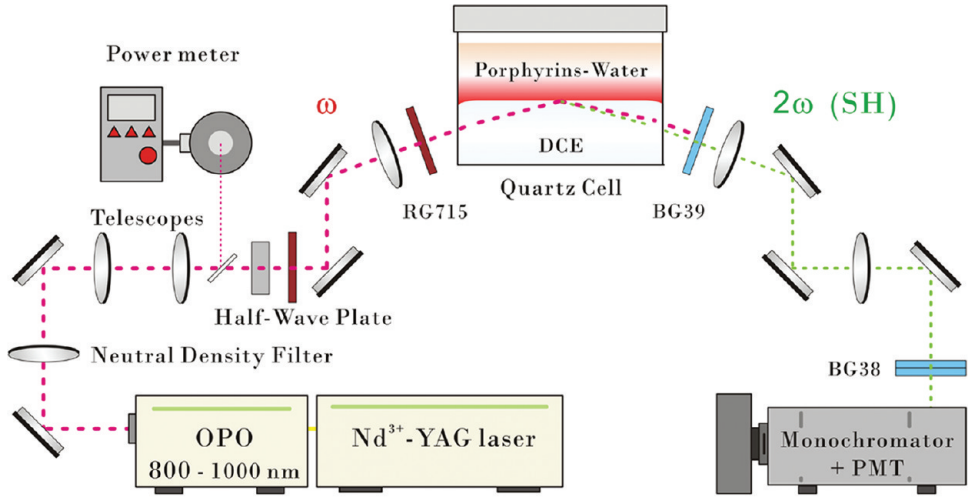

we have established that the lipophilic electron donor tetrathiafulvalene (TTF)[25−27] carries out the four-electron reduction of oxygen by the formation of a tetramer formed between neutral and protonated TTF.[28] However, the reaction needed around 10 h to complete at pH = 1. TTF, unlike Fc or DMFc, does not react with H_2O_2[28] allowing a more accurate quantification of the products of oxygen reduction.

The present work introduces the interfacial reduction of oxygen at ITIES by self-assembled oppositely charged water-soluble cobalt porphyrins, cobalt tetramethylpyridinium porphyrin ($CoTMPyP^{4+}$) and cobalt tetrasulphonatophenyl porphyrin ($CoTPPS^{4-}$). The catalytic activity of the interfacial self-assembled "raft" is surprisingly as good as, if not better, than the catalytic activity of synthetic Pacman cofacial porphyrins, when tested in the same conditions.

2. EXPERIMENTAL SECTION

2.1. Chemicals. All solvents and chemicals were used as received without further purification. Bis(triphenylphosphoranylidine)-ammonium chloride (BACl 98%), tetrakis(pentafluorophenyl)-borate ethyl etherate (LiTB purum) and lithium chloride (LiCl >99%) were purchased from Fluka. Chlorhydric acid (37−38%) and 1,2-dicholoroethane (DCE, grade HPLC) were purchased from Merck and Applichem respectively. Tetrathiafulvalene (TTF 99+%) was purchased from Acros and sodium iodide (NaI 98%) was purchased from Aldrich. The synthesis and characterization of Cobalt tetramethylpyridinium porphyrin ($CoTMPyP^{4+}$), cobalt tetrasulphonatophenyl ($CoTPPS^{4-}$), Co_2(DPOx), Co_2(DPO) and Co_2(DPX) is available in the Supporting Information (SI) online (see Section SI1 and Figures SI1, SI2 and SI3).

2.2. Optical Measurements. The UV−visible absorption spectra were recorded with a standard spectrophotometer (Ocean Optical, model Chem2000) using quartz cells with a path length of 10 or 1 mm.

Scheme 1 shows a diagram of the optical setup used for the SSHG measurements at the liquidlliquid interfaces. The fundamental beam is delivered by an Optical Parametric Oscillator (OPO) pumped by a nanosecond laser (Ekspla, model NT342B-10) delivering 108 mJ at 355 nm. The wavelength of the idler output from the OPO ranged between 800 and 1000 nm and the pulse duration is 3−5 ns. The weakly divergent idler output from the OPO is corrected with a slightly not-collimated telescope, formed by the combination of a diverging lens, focal length −75 mm, and a converging lens, focal length +150 mm. The linearly polarized collimated beam is passed through a neutral density filter in order to get 1 mJ of inlet power and a motorized half-wave plate is used to set the angle of polarization. In order to remove any SSHG radiation prior to the cell, three low-pass filters (Melles-Griot, model RG715) are placed on the beam path. Then, a converging lens, focal length +100 mm, focuses the fundamental beam onto the water|DCE interface from the organic phase. Total Internal Reflection (TIR) is achieved with an angle of incidence of about 70°. The reflected SSHG radiation is then separated from the fundamental beam with a high pass filter (Melles-Griot, model BG38). The collected SH signal is then collimated with two successive converging lenses with respective focal lengths +300 mm and +200 mm. Finally, the SH photons are detected through a monochromator (Jobin-Yvon, model HR320) with a photomultiplier tube (Hamamatsu, model R928). The SH radiation is further filtered with two successive filters (Melles-Griot, model BG38) before entering the monochromator. A power meter (Ophir, model PE-10) is used to continuously monitor the fundamental beam energy and the SHG signal was averaged over 300 laser shots. The resulting SSHG spectra were all corrected for background noise.

2.3. Ion-Transfer Voltammetry at ITIES. Ion-transfer voltammetry measurements at the water|DCE interface were performed in a four-electrode cell following the configuration described previously by Hatay et al.[20] A commercial potentiostat (PGSTAT 30, Metrohm, CH) was used. In the four-electrode cell two reference electrodes polarize the interface and two platinum counter electrodes provide the current. The external potential is applied by means of two silver/silver chloride (Ag/AgCl) reference electrodes, which are connected to the aqueous and DCE phases, respectively, by means of a Luggin capillary.[20] The Galvani potential difference $\Delta_o^w\phi$ was estimated by taking the formal ion transfer potential of TMA^+ as 0.18 V.[29] The schematic representation of the initial composition of the four-electrode cell is illustratd in Figure SI4 (SI).

2.4. Two-Phase Reactions. Two-phase reactions were performed in glass flasks with a volume of 4 mL (2 mL each phase) under stirring at 900 rpm. The composition of the cells is illustrated in Scheme 2

Scheme 2. Schematic Representation of the Initial Composition of the Aqueous Phase and the Organic Phase for the Biphasic Reactions[a]

50 μM P^{4+}, P^{4-}, $[P^{4+}/P^{4-}]$, $[H_2P^{4+}/H_2P^{4-}]$, $[P^{4+}/H_2P^{4-}]$, $[H_2P^{4+}/P^{4-}]$, Co_2(DPOX), Co_2(DPO) or Co_2(DPX)	1 mM TTF
pH 2 (HCl)	
10 mM LiTB	
Water	*DCE*

[a] P^{4+}, $CoTMPyP^{4+}$; P^{4-}, $CoTPPS^{4-}$; H_2P^{4+}, H_2TMPyP^{4+}; H_2P^{4-}, H_2TPPS^{4-}; $[x/y]$, equimolar mixture (50 μM each component).

dx.doi.org/10.1021/ja2087322 | J. Am. Chem.Soc. 2012, 134, 498−506

and all the experiments were performed with air-saturated solutions at room temperature (21 ± 2 °C). In order to perform the analysis after 1 h of reaction, the aqueous and organic solutions were isolated from each other. The organic phase was directly subjected to the UV−visible spectroscopy in order to confirm formation of the radical cation $TTF^{\bullet+}$ (1 mm optical path), while the aqueous phase was treated with NaI in excess (equivalent to 0.1 M) prior to the UV−visible spectroscopic measurement in order to detect the formation of I_3^- from the oxidation of I^- by H_2O_2 (10 mm optical path).

2.5. Scanning Electron Microscopy of the Self-Assembled Systems. The SEM samples were prepared by stirring a biphasic system (water|DCE) containing 50 μM $CoTMPyP^{4+}$ and 50 μM equimolar mixture of $CoTMPyP^{4+}$ and $CoTPPS^{4-}$ in the aqueous phase. Afterward, drops of the resulting emulsion were placed on a silicon film and allowed dry slowly at room temperature. Scanning electron microscopy (SEM) images were acquired using a Philips FEI XLF-30 microscope at 10 kV.

2.6. Computational Details. All calculations were carried out using Gaussian09.[30] Static first order hyperpolarizabilities of monomers were computed in the gas phase at the TPSS[31]/6-31G* level of theory using the finite difference method to numerically differentiate analytic polarizabilities. The increment of the intensity of electrostatic field in the numerical differentiation was 0.0003 au The geometries were optimized at the same level of theory. CPKS[32,33] calculations at the B3LYP[34,35]/6-31G* level of theory were performed for comparison and qualitatively confirmed the results. Neglecting rotations of the methyl and sulphonato groups, each studied monomer has seven different isomers related by rotations of the plane of the ring of the tetramethylpyridinium or tetrasulphonatophenyl substituents. Six of these seven isomers consist of three pairs of chiral isomers, related by the mirror symmetry. The electronic energies of all isomers differ by less than 1 kcal/mol and the hyperpolarizability tensor β is also not very strongly affected by the isomerization. Therefore only values for isomers of the D_2 symmetry are reported here. Due to the symmetry of these isomers, the hyperpolarizability tensor β has only one nonzero component β_{xyz} (if the coordinate axes are parallel to the Co−N bonds), which is reported below. [As symmetry constraints were not applied in our calculations, the remaining components of β (not reported here) are vanishing only approximately.]

For simplicity, the study of the feasibility of formation of self-assembled structures between the two oppositely charged porphyrins was made considering the simplest and smallest possible structure, a dimer. Geometries of dimers were optimized with the ωB97-XD density functional,[36] which is explicitly corrected for dispersion, and with the 6-31G* basis set. Loose displacement criterion was used in the geometry optimization of the oxygen bridged dimer, due to high flexibility of the molecule on the shallow doublet potential energy surface in the solvent (standard criteria were used for forces). Core electrons of cobalt (MDF-10[37]) and sulfur (MWB-10[38]) were described by the Stuttgart-Dresden quasirelativistic energy-averaged pseudopotentials. The original set of pseudo-orbitals for the sulfur atom was augmented by the appropriate polarization function (α_d(S) = 0.498[39]) in order to form a balanced basis set. Open-shell complexes were treated using the unrestricted formalism. The solvent effects were modeled using the IEF-PCM[40] variant of the implicit continuum model with the UAHF cavity.[41] Dielectric permittivity (ε = 78.35) and other parameters were set to mimic the water environment. In addition to using the implicit solvation model, the possibility that several water molecules may be "intercalated" between the porphyrin rings in the structure of the cofacial dimer was explored for the singlet state of neutral complex with bound oxygen using the explicit-implicit methodology. (The Co−Co distance is longer in the complex with bound oxygen and the oxygen atoms provide hydrogen-bonding sites inside the cofacial complex facilitating the "intercalation" of water.) Several structures of the implicitly solvated dimer with four explicit water molecules were explored. In the lowest energy structure found, all four explicit water molecules were in the outer shell of the dimer. Out of structures, which had some water molecules between the porphyrin rings, the structure with two water molecules in between and two water molecules outside had the lowest energy. At the CAM-B3LYP/6-31G* level, which was used for geometry optimizations using relaxed displacement criteria, the energy difference between both structures was ∼15 kcal/mol (16 kcal/mol with wB97XD/6-31G* single point). Therefore, only implicit solvation model was used to characterize other cofacial dimer structures. Similarly to calculations of hyperpolarizabilities, only isomers formed from monomers of the D_2 symmetry were studied here. Moreover, only the cofacial geometries were considered, thus the existence of more stable minima with different geometrical arrangements cannot be excluded. Bond dissociation energies (BDEs) were also computed at the ωB97-XD/6-31G* level of theory including the solvent model and were corrected for the basis set superposition error (BSSE) using the counterpoise procedure[42] following the first approach of ref 43. No contribution originating from the motion of nuclei (except for the deformation of geometries of fragments following the dissociation) was included in the BDEs.

3. RESULTS AND DISCUSSION

Chart 1 displays the chemical structures of the porphyrins $CoTMPyP^{4+}$ (P^{4+}) and $CoTPPS^{4-}$ (P^{4-}). Oxygen reduction

Chart 1. Chemical Structures of $CoTMPyP^{4+}$ (1) and $CoTPPS^{4-}$ (2)

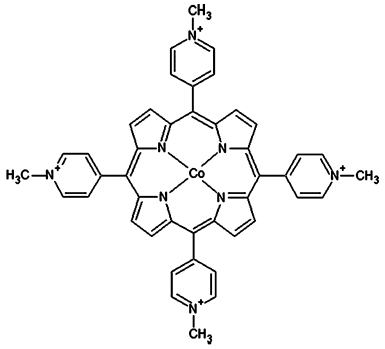

1

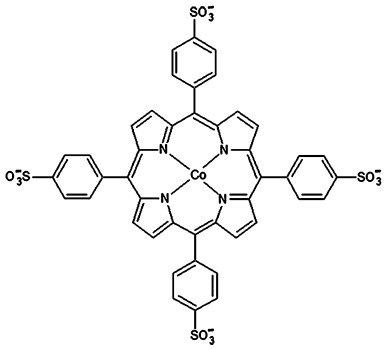

2

was carried out in air saturated solutions in the presence of one of the porphyrins or their equimolar mixture, hereafter written as [P^{4+}/P^{4-}], using the cell illustrated in Scheme 2. Tetrakispentafluorophenyl borate (TB^-) is initially present only in the aqueous phase, however, since it is a highly lipophilic anion, it transfers with a proton to the organic phase thereby polarizing the interface positively (water vs oil),[29] which favors the adsorption of both P^{4+} and [P^{4+}/P^{4-}]. As soon as both phases are in contact, the color of the organic phase changes from yellow to dark red associated to the oxidation of TTF to $TTF^{\bullet+}$[28] (Figure 1a). The evolution of signals at 343 nm, 439 and 582 nm in the UV−visible spectrum[27,28] of the organic phase after 1 h of

dx.doi.org/10.1021/ja2087322 | J. Am. Chem.Soc. 2012, 134, 498−506

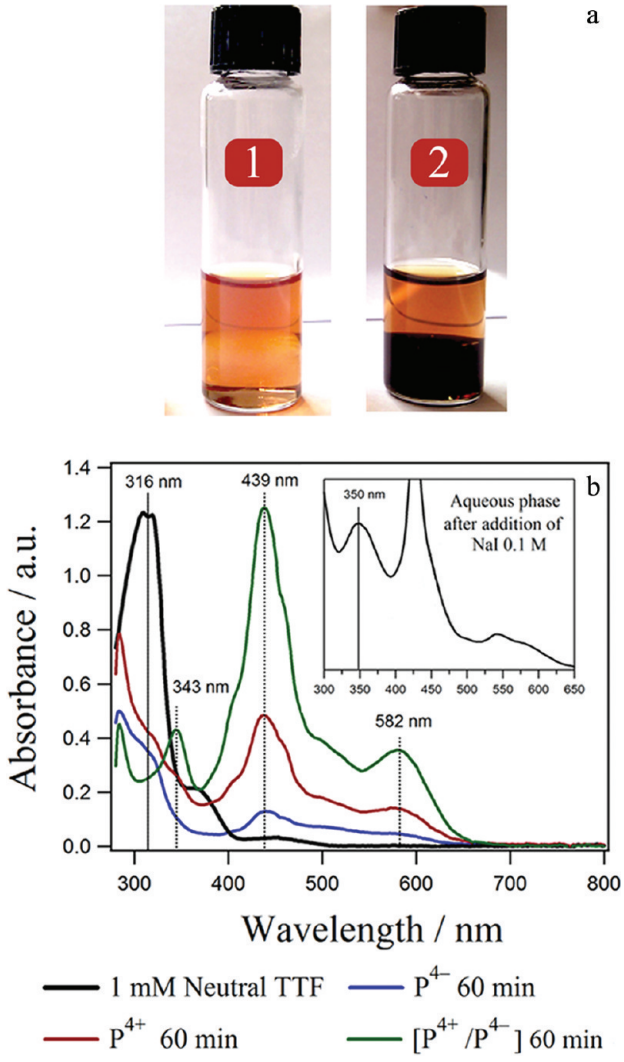

Figure 1. Catalytic activity results. (a) Photography of the cell before (1) and after 1 h of reaction (2). The color of the organic phase (bottom) immediately starts changing from yellow to red; (b) UV–visible absorption spectra of the organic phase after 1 h of biphasic reaction. (Inset) UV–visible spectrum of the aqueous phase after 1 h of reaction and treatment with 0.1 M NaI during 30 min. The peak at 350 nm corresponds to I_3^- obtained by the reaction between I^- and H_2O_2.

reaction (Figure 1b), confirms the formation of $TTF^{\bullet+}$. The results in Table 1 indicate that P^{4-} is a poor catalyst for oxygen reduction as shown by its low yield and selectivity toward H_2O, P^{4+} has intermediate activity and selectivity, while $[P^{4+}/P^{4-}]$ is an effective catalyst able to perform the direct four-electron reduction of oxygen with a selectivity of 78%. The fact that the catalytic activity of $[P^{4+}/P^{4-}]$ is not the linear combination of that of the isolated porphyrins, correlates with the behavior observed by UV–visible spectroscopy (Figure 2) where the Soret band of $[P^{4+}/P^{4-}]$ is significantly less intense and red-shifted with respect to the linear combination of the spectra of the isolated porphyrins, indicating that P^{4+} and P^{4-} are interacting to form a complex in water and more particularly at the interface, where the local relative permittivity can be considered equal to the half sum of the bulk values.[44]

In the present biphasic system, oxygen reduction can only occur at the interface where the adsorbed porphyrins are "sandwiched" between an excess of aqueous protons and lipophilic

Table 1. Catalytic Activity and Selectivity of the Isolated Porphyrins and the Self-Assembled System[a]

system	catalytic activity/%	selectivity toward H_2O_2/%	selectivity toward H_2O/%
P^{4-}	10	92	8
P^{4+}	36	45	55
$[P^{4+}/P^{4-}]$	96	22	78
H_2P^{4-}	N.A.	N.A.	N.A.
H_2P^{4+}	19	90	10
$[H_2P^{4+}/ H_2P^{4-}]$	17	92	8
$[H_2P^{4+}/P^{4-}]$	35	91	9
$[P^{4+}/ H_2P^{4-}]$	36	91	9
Co_2(DPOx)	100	37	63
Co_2(DPO)	100	39	61
Co_2(DPX)	100	25	75

[a]The catalytic activity was calculated with respect to the production of the radical cation $TTF^{\bullet+}$.[28] The selectivity towards H_2O was estimated from the production of H_2O_2, since those are the products of the reaction and it has been established that H_2O_2 neither reacts with TTF nor with protonated TTF.[28] P^{4+}, CoTMPyP^{4+}; P^{4-}, CoTPPS^{4-}; H_2P^{4+}, H_2TMPyP^{4+}; H_2P^{4-}, H_2TPPS^{4-}; [*x*/*y*], equimolar mixture (50 μM each component); N.A, Not-active.

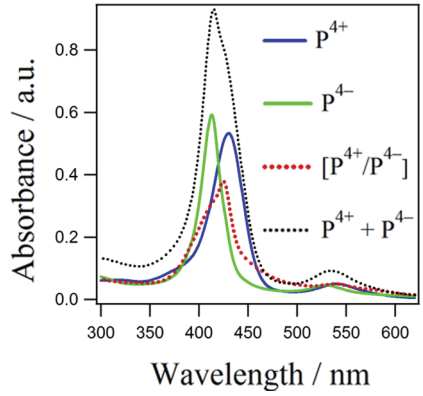

Figure 2. UV–visible spectra of 50 μM. P^{4+}, CoTMPyP^{4+}; P^{4-}, CoTPPS^{4-}; $[P^{4+}/P^{4-}]$, equimolar mixture of both porphyrins, and the linear combination of the absorption spectra of P^{4+} and P^{4-}.

electron donors. Thus, Surface Second Harmonic Generation (SSHG), a process in which two photons at a fundamental frequency are converted into one photon at the harmonic frequency, was used to characterize the adsorbed molecules and molecular "rafts". The second-order nonlinear susceptibility vanishes in the bulk of centrosymmetric media like liquids, therefore, SSHG is inherently selective for the interfacial species.[45−49]

For the SSHG measurements at the porphyrins-water|DCE interface the fundamental beam was linearly polarized *p* and *s*, that is, parallel and perpendicular to the plane of incidence respectively, and no analyzer was placed on the harmonic beam path. The *p* configuration yielded the largest SSHG intensities as shown in Figure 3. Figure 3 also gives the SSHG intensity recorded as a function of the fundamental beam angle of polarization γ. Those plots are used to get further insights into the origin of the SSHG process at the microscopic level. In this configuration, the SSHG intensity writes as:

$$I_{SSHG}(2\omega) = K[a\cos^2\gamma + b\sin^2\gamma + c\sin^2\gamma]^2 \quad (1)$$

dx.doi.org/10.1021/ja2087322 | J. Am. Chem.Soc. 2012, 134, 498–506

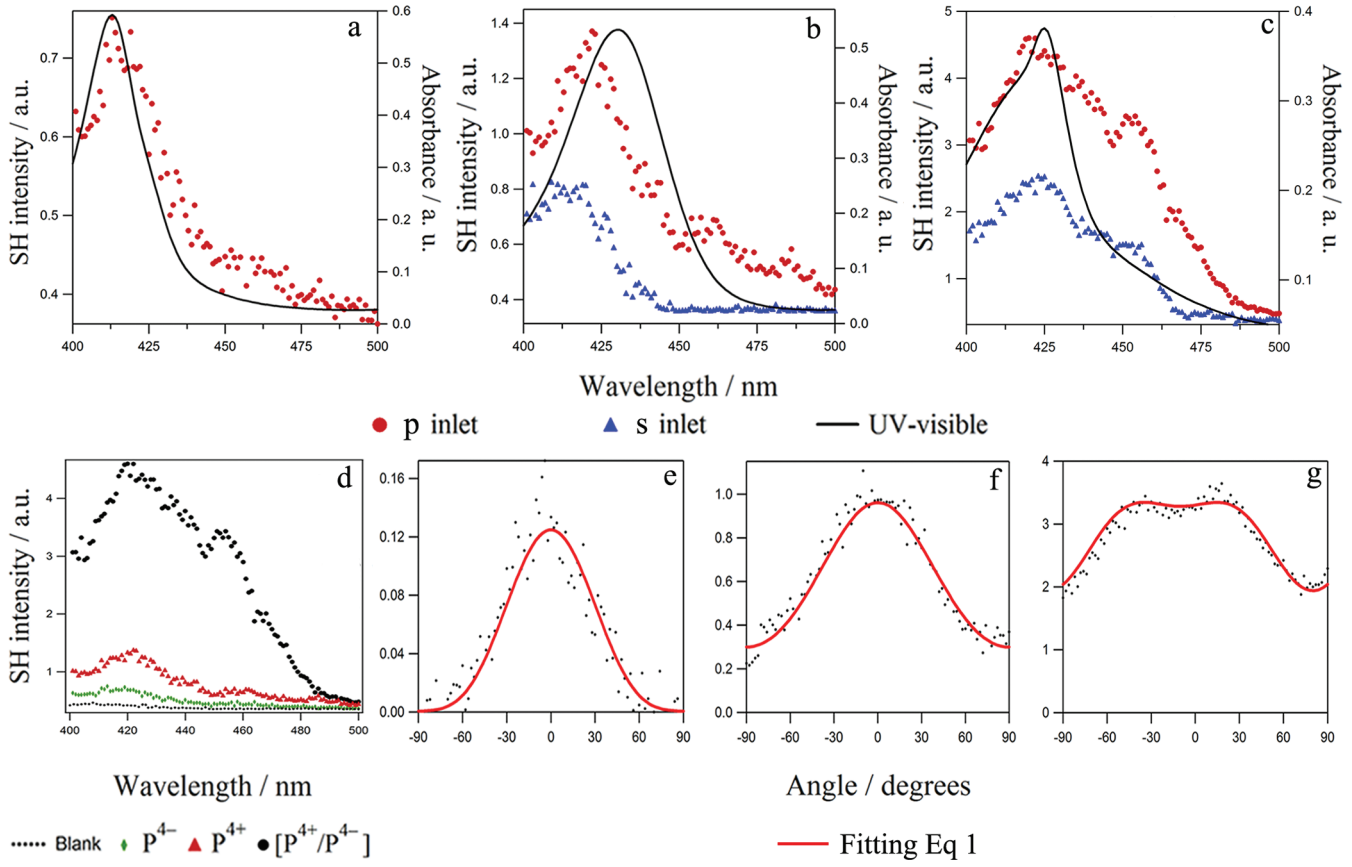

Figure 3. SSHG spectra of 100 μM of (a) P^{4-}, $CoTPPS^{4-}$; (b) P^{4+}, $CoTMPyP^{4+}$; (c) $[P^{4+}/P^{4-}]$, equimolar mixture of both porphyrins; (d) comparison between the SSHG spectrum of the three systems. Polarization angle dependence of the fundamental beam on the SSHG intensity for (e) P^{4-} ; (f) P^{4+}; (g) $[P^{4+}/P^{4-}]$.

where K is a general constant,ω is the frequency, and a, b and c are complex coefficients. These coefficients depend on the microscopic parameters describing the interface: the linear optical indices, the angle of incidence, the surface density of the porphyrins, their first hyperpolarizability at the interface and their orientation with respect to the interface, as described in the SI. The first hyperpolarizability of symmetrically substituted porphyrins is expected to be small in the bulk phase (100 au); however, small deviations of the porphyrin ring geometry from centrosymmetry and adsorption of the porphyrin at the interface can yield larger first hyperpolarizabilities. As a result, P^{4+}, P^{4-} and $[P^{4+}/P^{4-}]$ are easily observed by SSHG (Figure 3). In addition, if the porphyrins interact at the interface to form $[P^{4+}/P^{4-}]$, a much larger first hyperpolarizability is expected as compared to the single units P^{4+} and P^{4-}, owing to the two sets of positive and negative charges.

In Figure 3a, the SSHG spectrum of P^{4-} closely follows the UV−visible absorption spectrum recorded in bulk water, indicating that no major changes appear upon adsorption at the interface for P^{4-}. There is also no sign of aggregation and the solvatochromism is negligible. In contrast, the SSHG spectrum of P^{4+} (Figure 3b) exhibits clear changes as compared to the UV−visible absorption spectrum. By comparison with the UV−visible spectrum, the main resonance at 421 nm can be associated with the monomeric species and a small solvatochromic effect of about 10 nm is observed to the blue due to the presence of the organic phase. The red side of the resonance exhibits a shoulder at 460 nm, indicative of a weak aggregation process at the interface.

The most dramatic changes between the UV−visible spectrum and the second order process occur for the complex $[P^{4+}/P^{4-}]$ (Figure 3c). There is no solvatochromism of the main resonance but a strong shoulder on the red side of the spectrum, at around 450 nm is clearly observed. This feature indicates that the interaction of the anionic and cationic porphyrins into $[P^{4+}/P^{4-}]$ is reinforced at the interface due to the lower relative permittivity favoring ion pairing.

Calculations of the static first hyperpolarizability β of P^{4+} and P^{4-} monomers containing Co(II) centers (see the computational details) showed that the magnitude of β for P^{4+} (tensor element β_{xyz}= 2395 au, sign changes after rotation by 90°) is approximately 30% higher than the magnitude of β for P^{4-} (β_{xyz}= −1885 au, note the change of sign). The x, y and z indices stands for the molecular axes where x and y lies in the plane of the porphyrins rings and z perpendicular to them. Thus the fact that the SSHG signal of P^{4+} is 50% more intense than that of P^{4-}, can be accounted for by the change in the first hyperpolarizability magnitude. Furthermore, ion-transfer voltammetry at the polarized liquid−liquid interface (see Figure SI4, SI) showed that P^{4+} is more strongly adsorbed at the interface than P^{4-}, indicating that the larger SSHG intensity for P^{4+} compared P^{4-} stems from two concurring effects, that is, a higher first hyperpolarizability and a stronger adsorption.

The SSHG intensity for $[P^{4+}/P^{4-}]$ rafts is about 70% higher than that of P^{4+} and 84% than that of P^{4-}. This is due not only to an increase of the first hyperpolarizability, as expected from the molecular interaction, but also to higher packing at the interface resulting in an enhanced interfacial population.

dx.doi.org/10.1021/ja2087322 | J. Am. Chem.Soc. 2012, 134, 498−506

Therefore, by comparing the SSHG intensity for the three systems and taking into account the ion-transfer voltammetry results, it is possible to set a trend in terms of the number of adsorbed molecules at the interface as follow: $P^{4-} < P^{4+} < [P^{4+}/P^{4-}]$. This trend is similar to that established for the catalytic activity, indicating that the catalytic activity for interfacial oxygen reduction strongly depends on the adsorption of the catalyst at the interface. This observation further underlines that the reaction is mostly interfacial between dissolved oxygen, aqueous protons, adsorbed interfacial porphyrins and lipophilic sacrificial electron donors.

To characterize the interfacial self-assembly, the dependence of the SSHG intensity with the fundamental input angle of polarization was also determined at the fundamental wavelength of 842 nm, 828 nm, and 848 nm for P^{4-}, P^{4+} and $[P^{4+}/P^{4-}]$ respectively. Figure 3e, f and g shows that the behavior of $[P^{4+}/P^{4-}]$ is rather different from that of the isolated porphyrins. The SSHG intensity described by eq 1 has been fitted to estimate the coefficients *a*, *b* and *c*, see Table 2 and Figure 3e, f and g. The *a* coefficient is always the largest one and corresponds to the SSHG intensity collected with the fundamental beam *p* polarized at the interface. The main differences stems from the *c* parameter. A negligible value is determined for the monomeric species P^{4+} and P^{4-} whereas a negative value of −0.41 is obtained for $[P^{4+}/P^{4-}]$. It appears therefore that the monomeric species have similar nonlinear optical properties at the interface with modest differences between the relative values of their first hyperpolarizability tensor elements and possibly an orientational change as well. These SSHG results clearly show that the $[P^{4+}/P^{4-}]$ rafts possess an electronic structure remarkably different with respect to the isolated porphyrins and possibly a different interfacial orientation leading to a strong value of the *c* coefficient.

Table 2. Parameters obtained from the fitting of the polarization plots using eq 1[a]

species	*a*	*b*	*c*
P^{4-}	1	0.07	0
P^{4+}	1	0.55	0
$[P^{4+}/P^{4-}]$	1	0.77	−0.41

[a] P^{4+}: CoTMPyP^{4+}, P^{4-}: CoTPPS^{4-}, [*x*/*y*]: equimolar mixture (100 μM each component). The values are normalized with respect to the *a* coefficient. For simplicity, all parameters were assumed to retain a similar phase and were therefore taken as real values.

At this point, we can conclude that P^{4+} adsorbs at the interface to carry out oxygen reduction with a selectivity of 50% for the four-electron pathway whereas $[P^{4+}/P^{4-}]$ rafts strongly populate the interface and perform oxygen reduction very efficiently with a selectivity of 80%.

Secondary electron SEM images of $P^{4+}I_4^-$ and $[P^{4+}/P^{4-}]$ crystallized on a silicon substrate from a biphasic emulsion obtained by vigorous stirring are shown in Figure 4. Considering that the organic solvent is more volatile, the crystallization is likely to nucleate from adsorbed interfacial species. The images of $P^{4+}I_4^-$ obtained from the emulsion show microscale structures with a "leaf-like" asymmetric morphology (Figure 4a), while the crystals of $P^{4+}I_4^-$ obtained directly from water (see Figure SI5, SI) do not show such a defined morphology. This behavior corroborates the view that P^{4+} is adsorbed at the interface. The microstructures obtained from $[P^{4+}/P^{4-}]$ (Figure 4b) show a more complex "tree-like" morphology, and suggest that the $[P^{4+}/P^{4-}]$ rafts have a different molecular organization than the adsorbed P^{4+}.

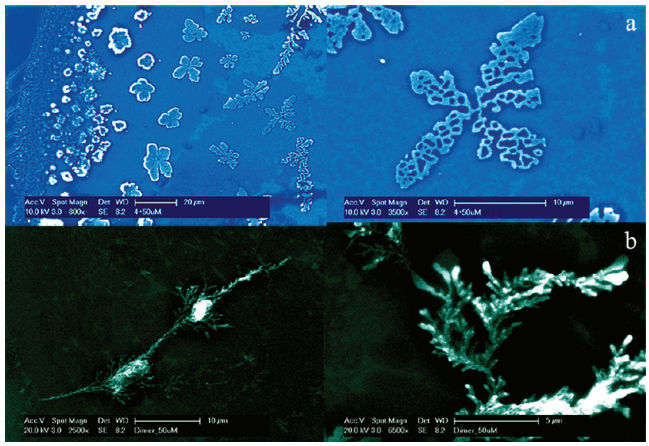

Figure 4. Secondary electron SEM images. (a) P^{4+}, CoTMPyP^{4+}; (b) $[P^{4+}/P^{4-}]$, equimolar mixture of both porphyrins taken at 10 kV.

To explain the high selectivity of the self-assembled $[P^{4+}/P^{4-}]$ toward the four-electron route, the three steps of the mechanism proposed for the four-electron reduction of oxygen by synthetic Pacman cofacial porphyrins must be considered:[1,5,8,50]

(i) Oxygen is held in the cavity formed between the two porphyrins.[1,5,8,50]

To determine whether in the complex $[P^{4+}/P^{4-}]$ both cobalt centers, from the P^{4-} and P^{4+} units, are involved in the catalytic activity, biphasic reactions were carried out using the free bases H_2P^{4+} and H_2P^{4-} and combinations thereof using the cell illustrated in Scheme 2. The results summarized in Table 2 and Figure SI6 (SI) clearly indicate that both cobalt centers are necessary to drive the four-electron reduction pathway by forming the μ-superoxo complex as in classical Pacman porphyrins.

(ii) The process $Co^{III}Co^{III}$ to $Co^{III}Co^{II}$ in the μ-superoxo complex is closely related to the dioxygen reduction and the distance between the two cobalt centers must be between 3 and 4 Å to stabilize the oxygen molecule and avoid its dissociation before the reduction is completed.[1,5]

The possibility of formation of a stable self-assembled complex $[P^{4+}/P^{4-}]$ with an appropriate Co−Co distance to perform the four-electron reduction of oxygen was confirmed by DFT calculations. However, only the cofacial dimer geometries were considered, thus the existence of more stable minima with different geometrical arrangements or oligomeration cannot be excluded. According to the reaction paths proposed in ref 5. the $[Co(III)TMPyP^{5+}/Co(III)TPPS^{3-}]^{2+}$ and $[Co(III)TMPyP^{5+}/Co(II)TPPS^{4-}]^{1+}$ charged dimers should be the most important for the reaction. The Co−Co distance calculated for $[Co(III)TMPyP^{5+}/Co(III)TPPS^{3-}]^{2+}$ (Figure 5a) is 3.93 Å (the distance is shorter by ∼0.5 Å in $[Co(III)TMPyP^{5+}/Co(II)TPPS^{4-}]^{1+}$), in agreement with the distance range proposed for four-electron reduction catalysts.[1,5] Stability of the 2+ charged dimer in the aqueous environment is further confirmed by the bond dissociation energy (BDE) of fragmentation of the dimer into $Co(III)TMPyP^{5+}$ and $Co(III)TPPS^{3-}$ monomers, which is equal to 41 kcal/mol. The 1+ charged dimer is slightly more stable and prefers dissociation into $Co(III)TMPyP^{5+}$ and $Co(II)TPPS^{4-}$, which is about

dx.doi.org/10.1021/ja2087322 | J. Am. Chem.Soc. 2012, 134, 498−506

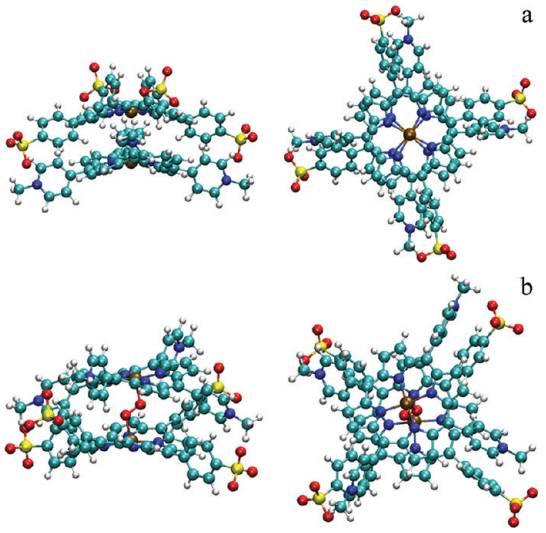

Figure 5. (a) Structure of the 2+ charged dimer formed between Co(III)TMPyP^{5+} and Co(III)TPPS^{3-}. Structures of the monomers in the dimer resemble structures of the monomers in the isolated (solvated) state, which exhibit the "rugged" (hyperbolic paraboloid) conformation of the porphyrin ring. The deformation energy of each monomer in the dimer is only ~4 kcal/mol. The ground state is a triplet and the spin density is localized on both porphyrin rings including Co atoms, but equal to zero in between them; (b) Structure of the μ-superoxo dimer formed between Co(III)TMPyP^{5+} and Co(II)TPPS^{4-}. Again, both monomers keep their "rugged" conformations, although more deformed than in the structure (a). The ground state is 1+ charged doublet with the spin density localized mostly on the oxygen atoms of the superoxide bridge. In both figures, the left panel shows a side view, parallel with the "planes" of the porphyrin rings, whereas the right panel shows a top view, perpendicular to the "planes" of the porphyrin rings.

~30 kcal/mol more advantageous than dissociation into Co(II)TMPyP^{4+} and Co(III)TPPS^{3-}. The structure of the 1+ charged doublet dimer with the oxygen molecule bound between the cobalt centers is shown in Figure 5b. Upon oxygen binding, the distance between cobalt centers increases to 4.41 Å. The distance between oxygen atoms, equal to 1.29 Å, and the spin density located on the central Co_2O_2 unit indeed correspond to a μ-superoxo bridge complex between two Co(III) centers, in accordance with the results obtained previously for the Pacman type porphyrins.[5]

(iii) The protonation of the μ-superoxo complex is necessary to allow reduction.[1,5,8,50]

Biphasic reactions between the porphyrins, the organic acid HTB (obtained by biphasic transfer between DCE and aqueous LiTB and HCl[28]) and TTF were performed in absence of protons in the aqueous phase. The results showed that in all cases the reaction was as slow as when the reaction is performed by TTF alone,[28] indicating that in the interfacial reaction, the protonation of the μ-superoxo complex by aqueous protons is a key step to reach the catalytic effect and provide more evidence that the reaction is interfacial.

The behavior of the porphyrins in presence of the supporting electrolytes LiTB and HCl was further studied. The UV–visible spectroscopy results show that in the bulk phase the behavior of the porphyrins strongly depends on the counterions. P^{4+} forms ion pairs with TB$^-$ in bulk (see Figure 6a), while P^{4-} and [P^{4+}/P^{4-}] associate with protons (see Figure 6b and c respectively). SSHG in Figure 6d showed that the addition of HCl and LiTB has no significant influence on the SSHG intensity of P^{4+}. However, a blue shift is observed in presence of LiTB indicating a weak association between aqueous TB$^-$ and P^{4+} at the interface.

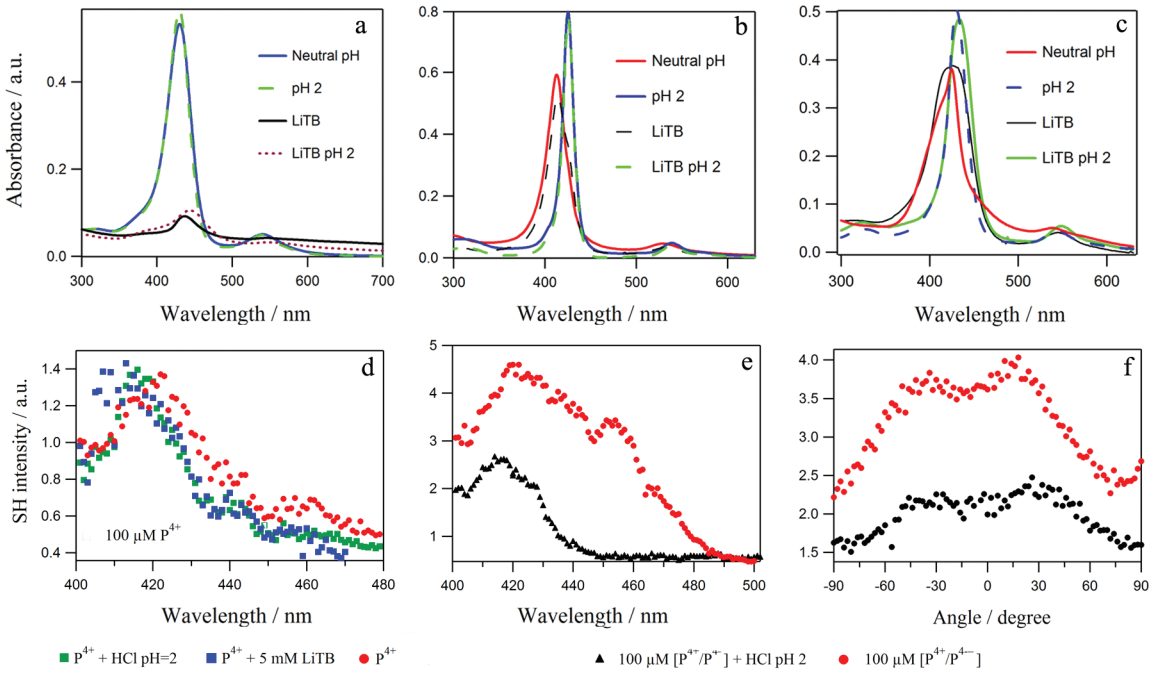

Figure 6. UV–visible absorption spectra and SSHG spectra of the porphyrins in presence of LiTB and HCl. (a) UV–visible spectrum of 50 μM CoTMPyP^{4+} (P^{4+}); (b) UV–visible spectrum of 50 μM CoTPPS^{4-} (P^{4-}); (c) UV–visible spectrum of 50 μM equimolar mixture of both porphyrins ([P^{4+}/P^{4-}]); (d) SSHG spectrum of 100 μM P^{4+}; (e) SSHG spectrum of 100 μM [P^{4+}/P^{4-}]; (f) Polarization angle dependence of the fundamental beam on the SSHG intensity for 100 μM [P^{4+}/P^{4-}].

dx.doi.org/10.1021/ja2087322 | J. Am. Chem.Soc. 2012, 134, 498–506

In contrast, the addition of protons promotes 20% decrease in the SSHG intensity of $[P^{4+}/P^{4-}]$ (see Figure 6e) due to the association between P^{4-} and protons that partially breaks down the assembly between P^{4+} and P^{4-}. However, the fundamental beam polarization angle dependence of the SSHG intensity did not change substantially (see Figure 6e), suggesting that the association in $[P^{4+}/P^{4-}]$ at the interface largely remains.

It has been claimed that in the bulk, the synthetic Pacman cofacial porphyrin Co_2(DPX) catalyzes the reduction of oxygen without forming H_2O_2 as a side product, by using ferrocene derivatives as electron donors.[51] However, ferrocene and its derivatives react with hydrogen peroxide, making the quantification of the products of the reaction uncertain. Therefore, the catalytic activity of the synthetic cofacial porphyrins Co_2(DPOx), Co_2(DPO) and Co_2(DPX) (see chemical structures in Figure SI7, SI), in the reduction of oxygen at the water|DCE interface, was tested using TTF as the lipophilic electron donor (see Scheme 2). Table 1 shows that the catalytic activity of Co_2(DPOx) and Co_2(DPO) is practically the same as the self-assembled system $[P^{4+}/P^{4-}]$, but the selectivity toward H_2O of the self-assembled system is around 12% higher. The catalytic activity and selectivity of Co_2(DPX) is practically the same as the complex $[P^{4+}/P^{4-}]$. This indicates that the self-assembled system reported in this work is at least as good as the synthetic cofacial porphyrins at the four-electron reduction of oxygen. Considering that the synthesis of cofacial porphyrins is an expensive and time-consuming process, this represents an important advantage from a technological point of view.

4. CONCLUSION

The interfacial four-electron reduction of oxygen by self-assembled oppositely charged water-soluble porphyrins rafts was demonstrated. Their catalytic activity is as good as that of synthetic cofacial porphyrins, proving that it is possible to perform such reaction in an efficient way, without the need of synthesizing cofacial porphyrins, a route that is expensive and tedious. This work is a clear example that it is possible to design molecular or supramolecular rafts to carry out selective reactions at liquidlliquid interfaces.

■ ASSOCIATED CONTENT

Ⓢ Supporting Information

Short explanation of SSHG, synthesis and characterization of the porphyrins, schematic representation of the four-electrode cell used for ion-transfer voltammetry and ion-transfer voltammograms of the porphyrins, secondary electrons SEM image of the cationic porphyrin crystallized directly from water, UV–visible spectra of the organic phase after biphasic reaction uisng mixtures of the free bases of the porphyrins and cobalt porphyrins as catalysts, chemical structures of the synthetic cofacial porphyrins, full name list of ref 30. This material is available free of charge via the Internet at http://pubs.acs.org.

■ AUTHOR INFORMATION

Corresponding Author

*hubert.girault@epfl.ch

■ ACKNOWLEDGMENTS

We thank the NCCR SNF MUST project, the EPFL and the "Centre National de la Recherche Scientifique" (CNRS, ICMUB, UMR 5260) for financial support. H.J.X. also acknowledges the "Région Bourgogne" and CNRS for a post-doctoral fellowship.

■ REFERENCES

(1) Collman, J. P.; Wagenknecht, P. S.; Hutchison, J. E. *Angew. Chem., Int. Ed. Engl.* **1994**, *33*, 1537–1554.
(2) Shi, C.; Steiger, B.; Yuasa, M.; Anson, F. C. *Inorg. Chem.* **1997**, *36*, 4294–4295.
(3) McGuire, R. Jr; Dogutan, D. K.; Teets, T. S.; Suntivich, J.; Shao-Horn, Y.; Nocera, D. G. *Chem. Sci.* **2010**, *1*, 411–414.
(4) Dogutan, D. K.; Stoian, S. A.; McGuire, R.; Schwalbe, M.; Teets, T. S.; Nocera, D. G. *J. Am. Chem. Soc.* **2010**, *133*, 131–140.
(5) Chang, C. J.; Loh, Z.-H.; Shi, C.; Anson, F. C.; Nocera, D. G. *J. Am. Chem. Soc.* **2004**, *126*, 10013–10020.
(6) Collman, J. P.; Denisevich, P.; Konai, Y.; Marrocco, M.; Koval, C.; Anson, F. C. *J. Am. Chem. Soc.* **1980**, *102*, 6027–6036.
(7) Collman, J. P.; Fu, L.; Herrmann, P. C.; Zhang, X. *Science* **1997**, *275*, 949–951.
(8) Durand, R. R. Jr; Bencosme, C. S.; Collman, J. P.; Anson, F. C. *J. Am. Chem. Soc.* **1983**, *105*, 2710–2718.
(9) Chen, J.; Zhang, W.; Officer, D.; Swiegers, G. F.; Wallace, G. G. *Chem. Commun.* **2007**, 3353–3355.
(10) Franco, R.; Jacobsen, J. L.; Wang, H.; Wang, Z.; Istvan, K.; Schore, N. E.; Song, Y.; Medforth, C. J.; Shelnutt, J. A. *Phys. Chem. Chem. Phys.* **2010**, *12*, 4072–4077.
(11) Tian, Y.; Martin, K. E.; Shelnutt, J. Y. T.; Evans, L.; Busani, T.; Miller, J. E.; Medforth, C. J.; Shelnutt, J. A. *Chem. Commun.* **2011**, *47*, 6069–6071.
(12) Medforth, C. J.; Wang, Z.; Martin, K. E.; Song, Y.; Jacobsen, J. L.; Shelnutt, J. A. *Chem. Commun.* **2009**, 7261–7277.
(13) Ogawa, K.; Kobuke, Y. *J. Photochem. Photobiol., C* **2006**, *7*, 1–16.
(14) Hasobe, T. *Phys. Chem. Chem. Phys.* **2010**, *12*, 44–57.
(15) Brewer, A.; Lacey, M.; Owen, J. R.; Nandhakumar, I.; Stulz, E. *J. Porphyr. Phthalocya.* **2011**, *15*, 257–263.
(16) Martin, K. E.; Wang, Z.; Busani, T.; Garcia, R. M.; Chen, Z.; Jiang, Y.; Song, Y.; Jacobsen, J. L.; Vu, T. T.; Schore, N. E.; Swartzentruber, B. S.; Medforth, C. J.; Shelnutt, J. A. *J. Am. Chem. Soc.* **2010**, *132*, 8194–8201.
(17) Chen, Z.; Lohr, A.; Saha-Möller, C. R.; Würthner, F. *Chem. Soc. Rev.* **2009**, *38*, 564–584.
(18) Hikal, W. M.; Harmon, H. J. *Polyhedron* **2009**, *28*, 113–120.
(19) Partovi-Nia, R.; Su, B.; Li, F.; Gros, C. P.; Barbe, J. M.; Samec, Z.; Girault, H. H. *Chem.—Eur. J.* **2009**, *15*, 2335–2340.
(20) Hatay, I.; Su, B.; Li, F.; Mendez, M. A.; Khoury, T.; Gros, C. P.; Barbe, J. M.; Ersoz, M.; Samec, Z.; Girault, H. H. *J. Am. Chem. Soc.* **2009**, *131*, 13453–13459.
(21) Su, B.; Hatay, I.; Trojanek, A.; Samec, Z.; Khoury, T.; Gros, C. P.; Barbe, J. M.; Daina, A.; Carrupt, P. A.; Girault, H. H. *J. Am. Chem. Soc.* **2010**, *132*, 2655–2662.
(22) Mendez, M.; Partovi-Nia, R.; Ge, P.; Olaya, A.; Hojeij, M.; Girault, H. H. *Phys. Chem. Chem. Phys.* **2010**, *12*, 15163–15171.
(23) Cunnane, V. J.; Geblewicz, G.; Schiffrin, D. J. *Electrochim. Acta* **1995**, *40*, 3005–3014.
(24) Trojánek, A.; Langmaier, J.; Samec, Z. *Electrochem. Commun.* **2006**, *8*, 475–481.
(25) Giffard, M.; Gorgues, A.; Riou, A.; Roncali, J.; Alonso, P.; Uriel, S.; GarÌn, J.; Nguyen, T. P. *Synt. Met.* **1995**, *70*, 1133–1134.
(26) Guldi, D. M.; Sanchez, L.; Martin, N. *J. Phys. Chem. B* **2001**, *105*, 7139–7144.
(27) Wudl, F.; Smith, G. M.; Hufnagel, E. J. *J. Chem. Soc., Chem. Commun.* **1970**, 1453–1454.
(28) Olaya, A. J.; Ge, P.; Gonthier, J. F.; Pechy, P.; Corminboeuf, C.; Girault, H. H. *J. Am. Chem. Soc.* **2011**, *133*, 12115–12123.
(29) Olaya, A. J.; Méndez, M. A.; Cortés-Salazar, F.; Girault, H. H. *J. Electroanal. Chem.* **2010**, *644*, 60–66.
(30) Frisch, M. J.; et al. *Gaussian 09*, Revision A.01; Gaussian Inc.: Wallingford CT, 2009.
(31) Tao, J.; Perdew, J. P.; Staroverov, V. N.; Scuseria, G. E. *Phys. Rev. Lett.* **2003**, *91*, 146401.

(32) Frisch, M.; Head-Gordon, M.; Pople, J. *Chem. Phys.* **1990**, *141*, 189−196.
(33) Johnson, B. G.; Fisch, M. J. *J. Chem. Phys.* **1994**, *100*, 7429−7442.
(34) Becke, A. D. *J. Chem. Phys.* **1993**, *98*, 5648−5652.
(35) Stephens, P. J.; Devlin, F. J.; Chabalowski, C. F.; Frisch, M. J. *J. Phys. Chem.* **1994**, *98*, 11623−11627.
(36) Chai, J.-D.; Head-Gordon, M. *Phys. Chem. Chem. Phys.* **2008**, *10*, 6615−6620.
(37) Dolg, M.; Wedig, U.; Stoll, H.; Preuss, H. *J. Chem. Phys.* **1987**, *86*, 866−872.
(38) Bergner, A.; Dolg, M.; Kuchle, W.; Stoll, H.; Preuss, H. *Mol. Phys.* **1993**, *80*, 1431−1441.
(39) Burda, J. V.; Zeizinger, M.; Šponer, J.; Leszczynski, J. *J. Chem. Phys.* **2000**, *113*, 2224−2232.
(40) Cancès, E.; Mennucci, B.; Tomasi, J. *J. Chem. Phys.* **1997**, *107*, 3032−3041.
(41) Barone, V.; Cossi, M.; Tomasi, J. *J. Chem. Phys.* **1997**, *107*, 3210−3221.
(42) Boys, S. F.; Bernardi, F. *Mol. Phys.* **1970**, *19*, 553−566.
(43) Zimmermann, T.; Chval, Z.; Burda, J. V. *J. Phys. Chem. B* **2009**, *113*, 3139−3150.
(44) Wang, H.; Borguet, E.; Eisenthal, K. B. *J. Phys. Chem. B* **1998**, *102*, 4927−4932.
(45) Fujiwara, K.; Monjushiro, H.; Watarai, H. *Chem. Phys. Lett.* **2004**, *394*, 349−353.
(46) Fujiwara, K.; Wada, S.; Monjushiro, H.; Watarai, H. *Langmuir* **2006**, *22*, 2482−2486.
(47) Conboy, J. C.; Richmond, G. L. *Electrochem. Acta* **1995**, *40*, 2881−2886.
(48) Nagatani, H.; Piron, A.; Brevet, P. F.; Fermin, D. J.; Girault, H. H. *Langmuir* **2002**, *18*, 6647−6652.
(49) Eugster, N.; Sreenivasan, K. P.; Su, B.; Girault, H. H. *Langmuir* **2006**, *22*, 1112−1120.
(50) Collman, J. P.; Hendricks, N. H.; Kim, K.; Bencosme, C. S. *J. Chem. Soc., Chem. Commun.* **1987**, 1537−1538.
(51) Fukuzumi, S.; Okamoto, K.; Gros, C. P.; Guilard, R. *J. Am. Chem. Soc.* **2004**, *126*, 10441−10449.

■ NOTE ADDED AFTER ASAP PUBLICATION

This article was published ASAP on December 15, 2011. One of the compounds in Scheme 2 was incorrect and has been updated. The corrected version was posted on December 19, 2011.